

Soft Matter

Accepted Manuscript



This is an *Accepted Manuscript*, which has been through the Royal Society of Chemistry peer review process and has been accepted for publication.

Accepted Manuscripts are published online shortly after acceptance, before technical editing, formatting and proof reading. Using this free service, authors can make their results available to the community, in citable form, before we publish the edited article. We will replace this *Accepted Manuscript* with the edited and formatted *Advance Article* as soon as it is available.

You can find more information about *Accepted Manuscripts* in the [Information for Authors](#).

Please note that technical editing may introduce minor changes to the text and/or graphics, which may alter content. The journal's standard [Terms & Conditions](#) and the [Ethical guidelines](#) still apply. In no event shall the Royal Society of Chemistry be held responsible for any errors or omissions in this *Accepted Manuscript* or any consequences arising from the use of any information it contains.



Using dynamic light scattering, we study orientational fluctuation modes in the nematic phase of a self-assembled lyotropic chromonic liquid crystal (LCLC) disodium cromoglycate and measure the Frank elastic moduli and viscosity coefficients. The elastic moduli of splay (K_1) and bend (K_3) are on the order of 10 pN while the twist modulus (K_2) is an order of magnitude smaller. The splay constant K_1 and the ratio K_1/K_3 both increase substantially as the temperature T decreases, which we attribute to the elongation of the chromonic aggregates at lower temperatures. The bend viscosity is comparable to that of thermotropic liquid crystals, while the splay and twist viscosities are several orders of magnitude larger. The temperature dependence of bend viscosity is weak. The splay and twist viscosities change exponentially with the temperature. In addition to the director modes, the fluctuation spectrum reveals an additional mode that is attributed to diffusion of structural defects in the column-like aggregates.

ARTICLE

Elasticity, Viscosity, and Orientational Fluctuations of a Lyotropic Chromonic Nematic Liquid Crystal Disodium Cromoglycate

Cite this: DOI: 10.1039/x0xx00000x

Received 00th January 2012,
Accepted 00th January 2012

DOI: 10.1039/x0xx00000x

www.rsc.org/

Shuang Zhou^{a,b}, Krishna Neupane^{c*}, Yuriy A. Nastishin^{a,d}, Alan R. Baldwin^c,
Sergij V. Shiyonovskii^{a,b}, Oleg D. Lavrentovich^{a,b,†} and Samuel Sprunt^{c,‡}

Using dynamic light scattering, we study orientational fluctuation modes in the nematic phase of a self-assembled lyotropic chromonic liquid crystal (LCLC) disodium cromoglycate and measure the Frank elastic moduli and viscosity coefficients. The elastic moduli of splay (K_1) and bend (K_3) are on the order of 10 pN while the twist modulus (K_2) is an order of magnitude smaller. The splay constant K_1 and the ratio K_1/K_3 both increase substantially as the temperature T decreases, which we attribute to the elongation of the chromonic aggregates at lower temperatures. The bend viscosity is comparable to that of thermotropic liquid crystals, while the splay and twist viscosities are several orders of magnitude larger. The temperature dependence of bend viscosity is weak. The splay and twist viscosities change exponentially with the temperature. In addition to the director modes, the fluctuation spectrum reveals an additional mode that is attributed to diffusion of structural defects in the column-like aggregates.

I. Introduction

Molecular self-assembly in solutions often results in anisometric aggregates capable of orientational order. The simplest examples are end-to-end “living polymerization”, formation of wormlike micelles by surfactants, and face-to-face stacking of disc-like molecules¹⁻⁸. In many systems, ranging from organic dyes and drugs^{1-3, 5} to DNA⁹, the aggregated polydisperse “building units” (Fig.1 (A)) form nematic and columnar phases, generally classified as lyotropic chromonic liquid crystals (LCLCs). Since the molecules in the aggregates are not covalently bound, the length of aggregates varies strongly with concentration, temperature, ionic content, etc., making the LCLCs very different from classic liquid crystals composed of molecules of fixed size and shape. Despite the growing interest in the LCLCs^{1, 9, 10}, little is known about their elastic and viscous properties. Knowledge of viscoelastic constants is of prime importance in understanding phenomena such as template-assisted alignment¹¹⁻¹⁴, behaviour of LCLCs in samples with various thickness¹⁵⁻¹⁷, LCLC-guided orientation

of nanoparticles¹⁸, shape of LCLC tactoids^{19, 20}, effect of spontaneously broken chiral symmetry^{21, 22}, and flow behaviour of LCLC²³.

There are two primary experimental techniques to determine the viscoelastic properties of nematic liquid crystals (LCs)²⁴: (1) the Frederiks transition, i.e., reorientation of the axis of nematic order (director) by an applied field, and (2) light scattering on thermal fluctuations of the director. The magnetic Frederiks transition has been applied to explore the elastic properties of two LCLCs, disulphoindantrone^{25, 26} and sunset yellow (SSY)²⁷. The Frederiks approach requires the LC director to be uniformly aligned in two different fashions, planar and homeotropic, with the director parallel to the bounding substrates of the sample cell and perpendicular to them, respectively. Such a requirement is difficult to satisfy for lyotropic systems. In particular, homeotropic anchoring of LCLCs has been reported only for a few cases^{17, 27, 28}. One of the most studied LCLCs, representing water dispersions of disodium cromoglycate (DSCG), shows only transient

homeotropic alignment (although there is a recent report on the homeotropic alignment at a graphene substrate²⁸), thus making it difficult to determine the viscoelastic properties of this material. On the other hand, knowledge of viscoelastic properties of DSCG is of particular importance for further understanding of LCLCs, since DSCG is optically transparent and has been used as a biocompatible component in real-time biological sensors²⁹ and in formulations of LCLC-bacterial dispersions³⁰⁻³².

In this paper, in order to characterize the material parameters of the nematic phase of water solutions of DSCG, we use the dynamic light scattering (DLS) that requires only one type (planar) of surface anchoring. The approach is similar to the one used previously by Meyer et al to characterize polymer solutions exhibiting the nematic phase^{8, 24, 33-36}, and allows one to extract both the elastic moduli and the viscosity coefficients. By calibrating the set-up with the measurement of DLS spectrum for the well-studied nematic 4'-n-pentyl-4-cyanobiphenyl (5CB), we extract the absolute values of the elastic constants and viscosities for DSCG. The approach allows us to trace both the concentration and temperature dependences of these viscoelastic parameters. A small portion of these results (one concentration only) were made available in 2008 in electronic-Liquid Crystal Communications³⁷ and arXiv³⁸.

In these measurements, we observe that the splay elastic constant K_1 , splay and twist viscosities η_{splay} and η_{twist} all increase dramatically as the temperature is reduced. The DLS spectrum not only shows the modes that correspond to the standard viscoelastic response (director modes), but also reveals an additional fluctuation mode weakly coupled to the director. We suggest that this mode is associated with structural defects in packing of chromonic aggregates such as stacking faults. The observed peculiarities of viscoelastic properties of LCLCs, absent in other LCs, originate from the fact that the chromonic molecules in the aggregates are bound by weak non-covalent interactions. As a result, the length of aggregates and the viscoelastic parameters that depend on it are extremely sensitive to both concentration and temperature.

II. EXPERIMENTAL DETAILS

Disodium Cromoglycate (DSCG), Fig. 1(A), was purchased from Spectrum Chemicals (98% purity) and subsequently dissolved in deionized water (resistivity 18 M Ω cm) at concentrations of $c=12.5, 14.0, 16.0$ and 18.0 wt%. Following Ref¹⁰, the corresponding volume fractions are: $\phi = 0.089, 0.100, 0.115,$ and 0.129 . The transition temperatures of the nematic to nematic-isotropic biphasic region are $T_{ni} = 297.0 \pm 0.2\text{K}, 299.6 \pm 0.4\text{K}, 303.5 \pm 0.3\text{K}$ and $306.2 \pm 0.2\text{K}$,

respectively, according to the established phase diagram³⁹ and our independent microscopy analysis. The DLS measurements were performed in the homogeneous nematic phase over the temperature range from 294.5K to within 1K of T_{ni} . The nematic director was aligned in a planar fashion by glass substrates coated with buffed layers of polyimide SE-7511 (Nissan Chemical Inc.)¹⁹. Optical cells of thickness 19 μm were sealed with epoxy to prevent water evaporation from the samples. The value of T_{ni} of each sample was checked before and after the measurement, showing changes of less than 1K in all cases. For light scattering measurements, the samples were housed in a hot stage with optical access and temperature control with an accuracy of 0.1 K and stability of 0.01 K over 1 hr.

The thermotropic nematic liquid crystal 4'-n-pentyl-4-cyanobiphenyl (5CB), used for reference measurements, was purchased from Sigma-Aldrich (98 % purity). Planar alignment of the director in a 13.7 μm thick sample is produced by buffed polyimide PI2555 layers (HD Microsystems) applied to surfaces of the flat glass substrates.

In the two studied light scattering geometries, the director $\hat{\mathbf{n}}$ is either perpendicular (geometry "1&2", Fig 1(B)) or parallel (geometry "3", Fig 1(C)) to the scattering plane. The polarization ($\hat{\mathbf{i}}$) of the normally incident $\lambda = 532$ nm laser light is vertical; depolarized scattering was collected through a horizontal analyzer ($\hat{\mathbf{s}}$). The laser power was kept below 3 mW to avoid parasite effects of light absorption. Homodyne cross-correlation functions of the scattered light intensity (evenly split between two independent detectors) were recorded as a function of time on a nanosecond digital correlator. The angular-dependent average light intensity $I_{1\&2}(\theta)$ (divided by the incident light intensity I_0 in the sample) measured in geometry "1&2" may be expressed as⁴⁰:

$$I_{1\&2} = I_1(\theta) + I_2(\theta) = (\Delta\varepsilon)^2 (\pi\lambda^{-2})^2 \Omega d A k_B T \left[\frac{G_1(\theta)}{K_1 q_{\parallel}^2(\theta)} + \frac{G_2(\theta)}{K_2 q_{\perp}^2(\theta)} \right] \quad (1)$$

where θ is the laboratory scattering angle, Ω is the collection solid angle, A is the cross-sectional area and d the thickness of the illuminated sample volume, $\Delta\varepsilon = \varepsilon_{\parallel} - \varepsilon_{\perp} = n_{\parallel}^2 - n_{\perp}^2$ is the dielectric anisotropy at optical frequency, n_{\parallel} and n_{\perp} are the refractive indices for light polarized parallel and perpendicular to the director, respectively, and $q_{\parallel}(\theta)$ and $q_{\perp}(\theta)$ are the two components of scattering vector $\mathbf{q} = \mathbf{k}_s - \mathbf{k}_i$ along and perpendicular to $\hat{\mathbf{n}}$ respectively. The geometrical scattering factors $G_1(\theta)$ and $G_2(\theta)$ are:

$$G_1(\theta) = \frac{\cos^2 \frac{\theta}{2} (1+p)^2}{1+p+s^2}, G_2(\theta) = \frac{\left(\sin \frac{\theta}{2} - s \cos \frac{\theta}{2} \right)^2}{1+p+s^2} \quad (2)$$

where $s = \frac{\Delta n}{2n_{\perp} \sin \frac{\theta}{2}}$, $p = \frac{\Delta n}{n_{\perp}}$, and $\Delta n = n_{\parallel} - n_{\perp}$ is the optical

birefringence of the LCLC sample. The separation of $I_1(\theta)$ and $I_2(\theta)$ is done by fitting the time correlation function of the scattered intensity $I_{1&2}(\theta)$ to two overdamped decay processes with different relaxation rates Γ_1 and Γ_2 (as discussed below).

The expression for the scattered intensity in geometry “3” is:

$$I_3(\theta) = (\Delta\varepsilon)^2 (\pi\lambda^{-2})^2 \Omega d A k_B T \frac{G_3(\theta)}{K_3 q_{\perp}^2(\theta) + K_2 q_{\perp}^2(\theta)} \quad (3)$$

where $G_3(\theta) = \cos^2 \theta$. In DSCG LCLC, as we will confirm below, $K_2 \ll K_3$. Over the range of angles $\theta = (5-35)^\circ$ studied, we estimate $\left(\frac{K_2 q_{\perp}^2}{K_3 q_{\perp}^2}\right)_{\max} \approx 0.01$. Thus we neglect $K_2 q_{\perp}^2$ in Eq.(3), leading to:

$$I_3(\theta) = (\Delta\varepsilon)^2 (\pi\lambda^{-2})^2 \Omega d A k_B T \frac{G_3(\theta)}{K_3 q_{\perp}^2(\theta)} \quad (4)$$

The cell gap (sample thickness) d was measured by interferometry in empty cells.

The measured intensities $I_{1,2,3}$ are functions of material parameters such as $\Delta\varepsilon$ and K 's, and experimental conditions such as d and T . To obtain absolute values of K_3 , we calibrated the scattered intensity ($I_3(\theta)$) measured on DSCG LCLC against measurements made in the identical geometry “3” set-up on a reference 5CB sample, whose values of $\Delta\varepsilon$, K_2 and K_3 are well known⁴¹⁻⁴³. We can then deduce the absolute values of the DSCG elastic constant K_3 from the ratio

$$\frac{[I_3(\theta)]_{DSCG}}{[I_3(\theta)]_{5CB}} = \frac{[K_3 q_{\perp}^2 + K_2 q_{\perp}^2]_{5CB} [G_3(\theta)(\Delta\varepsilon)^2 T d]_{DSCG}}{[K_3 q_{\perp}^2]_{DSCG} [G_3(\theta)(\Delta\varepsilon)^2 T d]_{5CB}} \quad (5)$$

and the values of K_1 and K_2 from similar ratios for $I_1(\theta)$ and $I_2(\theta)$.

From measurements of the homodyne intensity correlation function in time (τ), we obtain the angular dependent relaxation rates $\Gamma_{\alpha}(\theta)$ for the director fluctuations by fitting the experimental data in Fig. 2 to the standard expression for overdamped modes:

$$\langle I(0, \theta) I(\tau, \theta) \rangle = \bar{I}^2(\theta) + g^2 \left[\sum_{\alpha} \bar{I}_{\alpha}(\theta) \exp(-\Gamma_{\alpha} \tau) \right]^2 \quad (6)$$

Here g is the optical coherence factor⁴⁴. For geometry “1&2”, $\alpha = 1, 2$, the splay and twist modes contribute separately to the total

intensity; for geometry “3”, $\alpha = 3$, from Eq. (4) only the bend mode should contribute to the total intensity. From $\Gamma_{\alpha}(\theta)$, we obtain the corresponding orientational viscosities as: $\eta_{splay} = K_1 q_{\perp}^2(\theta) / \Gamma_1(\theta)$, $\eta_{twist} = K_2 q_{\perp}^2(\theta) / \Gamma_2(\theta)$ and $\eta_{bend} = K_3 q_{\perp}^2(\theta) / \Gamma_3(\theta)$.

III. RESULTS

A. Elastic constants

The temperature and concentration dependences of the elastic moduli K_1 , K_2 and K_3 of the nematic phase of DSCG are shown in Fig 3. The splay constant K_1 and bend constant K_3 are comparable to each other, being on the order of 10 pN, while the twist constant K_2 is about 10 times smaller (confirming the estimate leading to Eq.(4)). Similar values and large anisotropy were recently reported for another LCLC, Sunset Yellow²⁷. All three elastic moduli increase as the temperature T decreases, but K_1 shows a much steeper dependence than that of K_2 and K_3 . For example, for $c=18$ wt%, K_1 increases by a factor of 9 within a ~ 10 K temperature decrease, while K_2 increases only 3 fold and K_3 less than 2 fold. The temperature dependence of K_1 follows a universal exponential law for all concentrations

$$K_1(T) \propto \exp(-\beta_K T) \quad (7)$$

where $\beta_K = 0.20 \pm 0.01 \text{ K}^{-1}$ is independent of concentration, Fig 3(A).

The anisotropy of the elastic moduli is further illustrated in Fig 4 where the ratios of elastic constants are plotted as a function of T for different concentrations. When T decreases, both K_1 / K_3 and K_1 / K_2 increase. K_3 / K_2 remains practically constant (35 ± 5) over a wide temperature range for $c = 12.5, 14, 16$ wt%, whereas for $c = 18$ wt%, the value slightly decreases to about 25 at $T \approx 294$ K.

B. Viscosities

The concentration and temperature dependences of viscosities η_{splay} , η_{twist} and η_{bend} are shown in Fig 5. The viscosities η_{splay} and η_{twist} are comparable to each other and are in the range of (1 - 500) $\text{kgm}^{-1}\text{s}^{-1}$, several orders of magnitude larger than $\eta_{bend} = (0.007 - 0.03) \text{ kgm}^{-1}\text{s}^{-1}$. η_{splay} and η_{twist} show very strong temperature dependences, changing by over two orders of magnitudes when the temperature changes by only about 10K, Fig 5(A)(B). For the same temperature range, η_{bend} changes by a factor of 3 only, Fig 5(C). The temperature dependence of η_{splay} and η_{twist} are described by the exponential laws

$$\eta_{\text{splay}}(T) \propto \exp(-\beta_s T), \quad \eta_{\text{twist}}(T) \propto \exp(-\beta_t T) \quad (8)$$

where the concentration independent coefficients are $\beta_s = 0.41 \pm 0.02 \text{ K}^{-1}$, $\beta_t = 0.37 \pm 0.01 \text{ K}^{-1}$. Note that β_s and β_t are roughly twice as large as β_K .

The ratio $\eta_{\text{splay}}/\eta_{\text{twist}}$ slowly increases with T , Fig 5(D). In the vicinity of nematic to nematic-isotropic biphasic transition (low concentrations or small ΔT), $\eta_{\text{splay}}/\eta_{\text{twist}}$ remains close to 1 within the accuracy of experiments. Deeper into the nematic phase (and specifically for the highest concentration $c = 18 \text{ wt}\%$ and for $\Delta T \approx 12 \text{ K}$), $\eta_{\text{splay}}/\eta_{\text{twist}}$ increases to about 2.

C. An additional mode in bend geometry

As indicated by Eqs. (1) and (6), two modes, namely pure splay and pure twist, contribute separately to the total intensity in the “1&2” scattering geometry. The corresponding correlation function should

reveal two relaxation processes with $\Gamma_1(\theta) = \frac{K_1 q_{\perp}^2(\theta)}{\eta_{\text{splay}}}$,

$\Gamma_2(\theta) = \frac{K_2 q_{\perp}^2(\theta)}{\eta_{\text{twist}}}$. This is indeed what we obtain by fitting

experimental data, as indicated in Fig 2. On the other hand, Eqs.(4) and (6) predict that bend fluctuations contribute to the intensity in geometry “3”, and thus the correlation function should show a single

relaxation process with $\Gamma_3(\theta) = \frac{K_3 q_{\perp}^2(\theta)}{\eta_{\text{bend}}}$. However, fitting the

experimental data with a single exponential decay fails to match the data, Fig 2. A minimum of two relaxation modes, with a stretching exponent $b = 0.9$, are needed to fit the correlation data:

$$\langle I(0, \theta) I(\tau, \theta) \rangle = \bar{I}^2(\theta) + g^2 \left[\bar{I}_3(\theta) \exp\left(-\frac{K_3 q_{\perp}^2}{\eta_{\text{bend}}} \tau\right)^b + \bar{I}_4(\theta) \exp(-\Gamma_4 \tau)^b \right]^2 \quad (9)$$

Fits of the data in geometry “3” to Eq. (9) indicate $\Gamma_4 \propto q_{\perp}^2$, thus the additional mode is hydrodynamic. The fact that b is close to 1 implies that the relaxation rates do not have single values but show narrow dispersion⁴⁵. Since $I_4/I_3 \approx 0.1$, the presence of the additional mode does not increase the uncertainty in the values deduced for K_3 and η_{bend} by more than 10%; the other viscoelastic parameters (measured in geometry “1&2”) are unaffected.

IV. DISCUSSION

The LCLC DSCG shows some unique features as compared to conventional thermotropic nematics such as 5CB and to other nematic lyotropic LC systems, including the LCLC SSY and nematic polymeric LCs such as poly(γ -benzyl glutamate)(PBG), Table 1, Fig 2-5. First, the anisotropy of the elastic constants of DSCG is the largest among all the representative nematics shown in Table 1. The twist constant (K_2) is more than 10 times smaller than the splay (K_1) and bend

(K_3) constants, while the latter two are comparable to each other, Fig. 4(A). Second, K_1 has a much stronger (exponential) temperature dependence as compared to the linear dependences of K_2 and K_3 . Third, the DSCG viscosities associated with splay and twist deformation, η_{splay} and η_{twist} , are both anomalously large, 3-5 orders of magnitude larger than the bend viscosity η_{bend} of DSCG and the viscosities measured in thermotropic LCs such as 5CB (which are on the order of $0.01 \text{ kgm}^{-1} \text{ s}^{-1}$). Fourth, the temperature dependence of the parameters K_1 , η_{splay} and η_{twist} can be described by concentration-independent exponential laws, Eq.(7)(8) with the exponents $\beta_K = 0.2$, $\beta_s = 0.41$ and $\beta_t = 0.37$, respectively.

We now proceed to discuss our results in terms of relevant theoretical models for viscoelastic properties of lyotropic nematics.

A. Elastic constants

The viscoelasticity of lyotropic systems is usually described by the Onsager type models^{35, 46-48} based on the idea of excluded volume. In the simplest version, the building units are considered as long slender rods with the length-to-diameter ratio L/D being fixed and much larger than 1. The nematic ordering is caused by the increase of concentration; the rods sacrifice orientational freedom to maintain the ability to translate. The model is athermal as the behaviour is controlled exclusively by entropy. The excluded volume theory predicts the elastic constants in a system of rigid long rods⁴⁷ as follows:

$$K_1 = \frac{7}{8\pi} \frac{k_B T}{D} \phi \frac{L}{D}, \quad K_2 = K_1 / 3 \quad \text{and} \quad K_3 = \frac{4}{3\pi^2} \frac{k_B T}{D} \phi^3 \left(\frac{L}{D}\right)^3.$$

Clearly, this model does not describe our experimental findings for the LCLC system well. For example, the measured K_1/K_2 can be as high as ~ 30 ($c = 18 \text{ wt}\%$, $T \approx 294 \text{ K}$), Fig. 4(B), much larger than the expected constant value of 3. Furthermore, to form a nematic phase, the system of rigid rods should be of a volume fraction that exceeds a critical value $\phi_c = 4.5D/L$ ⁴⁰. If

that is the case, then one would expect $\frac{K_3}{K_1} \approx \frac{1}{2} \phi^2 \left(\frac{L}{D}\right)^2 > 10$,

while our experiment yields a much lower value $\frac{K_3}{K_1} \ll (1-3)$ in nematic DSCG, Fig 4(A).

To explain the smallness of K_2 , one may consider effects such as the electrostatic interaction of charged rods⁴⁶, since the dissociation of ionic groups into water from the periphery of the DSCG aggregates makes them charged. However this correction turns out to be negligible. Coulomb repulsion of similarly charged cylinders tends to arrange them perpendicularly to each other. This “twisting effect” thus modifies K_2 by a factor⁴⁶ $\approx (1 - 0.1h)$, where $h = \lambda_D / (D + 2\lambda_D)$, $D \approx 1.6 \text{ nm}$ is the “bare” diameter of DSCG aggregates³⁹ and

λ_D is the Debye screening length. For the DSCG solutions used in this work, $\lambda_D \approx 0.5 \text{ nm}^{49}$. Therefore, the twisting effect might lead to a decrease of K_2 by only a few percent, and is most likely not the main reason for the observed smallness of K_2 . The situation is very similar to the one recently discussed for LCLC Sunset Yellow²⁷.

The next level of theoretical modelling is to take into account that the aggregates comprising the LCLC are not absolutely rigid but possess some flexibility^{33, 47, 48}, characterized by a finite persistence length λ_p , that should directly affect K_3 . The persistence length is a measure of the length scale over which the unit vectors tangential to the flexible elongated object lose their correlations. Flexibility of LCLC aggregates is evident in recent numerical simulations^{50, 51} and suggested by recent nuclear magnetic resonance measurements, where column undulation within the molecular stack involving 4-8 molecules was observed⁵².

When the aggregates are flexible, the bend deformation is no longer inhibited by their length; each aggregate can bend to follow the director pattern, Fig. 6(A). According to the well-known result of the elastic theory^{53, 54}, the bending energy of an elastic rod is $F_3 = \frac{1}{2} \kappa L \rho^2$, where κ is the bending stiffness and ρ is the curvature of the bent rod. The volumetric elastic energy density for a dispersion of elastic rods is then³⁵ $f_3 = F_3 \phi \left(\frac{\pi}{4} D^2 L \right)^{-1}$. Using the relationships between the persistence length λ_p and bending stiffness⁵³, $\lambda_p = \kappa / k_B T$, and between the energy density of bend and K_3 , $f_3 = \frac{1}{2} K_3 \rho^2$, one arrives at

$$K_3 = \frac{4 k_B T}{\pi D} \phi \frac{\lambda_p}{D} \quad (10)$$

The last result is twice as large as the expression derived by Taratuta et al.³⁵, who defined λ_p as $\frac{2\kappa}{k_B T}$. Equation(10) with the typical experimental values $K_3 = 10 \text{ pN}$, $\phi = 0.1$ and $D = 1.6 \text{ nm}$ ³⁹ yields an estimate $\lambda_p = 50 \text{ nm}$. This value is close to the persistence length of double-stranded DNA (dsDNA)⁹, which has structural parameters similar to the aggregate of DSCG (diameter $\sim 2 \text{ nm}$ and 6 ionizable groups per 1 nm of length).

The value of K_3 for DSCG at $\phi \approx 0.1$ is several times larger than the value $K_3 = 6.1 \text{ pN}$ reported for SSY²⁷ with $\phi \approx 0.20$, Table 1. To discuss the difference, it is convenient to represent the bending stiffness of the chromonic aggregate through the Young's modulus Y of a homogeneous elastic cylinder⁵³: $\kappa = \pi Y D^4 / 64$. Therefore,

$$K_3 = \frac{\phi Y D^2}{16} \quad (11)$$

The aggregates in the DSCG LCLC have a larger cross section⁵⁵ ($D^2 \sim 2.4 \text{ nm}^2$) than those for SSY⁵⁵ ($D^2 \sim 1.2 \text{ nm}^2$), so that the product ϕD^2 in Eq. (11) is essentially the same for the two LCLCs. Hence, the difference in the values of K_3 can be attributed to the difference in the Young modulus Y , which is worthy of further investigation. When $K_3 = 10 \text{ pN}$, Eq.(11) leads to $Y = 6.7 \times 10^8 \text{ N/m}^2$, which is the same order of magnitude as the sequence dependent Young's modulus for dsDNA⁵⁶ (for example, $Y \approx 3 \times 10^8 \text{ N/m}^2$ for the λ -phage dsDNA⁵⁷).

The flexibility of aggregates does not affect the splay constant K_1 much. As explained by Meyer⁸, splay deformations, under the condition of constant density, limit the freedom of molecular ends, which decreases the entropy, Fig. 6(B). A larger contour length L implies a smaller number of molecular ends available to accommodate for splay and thus a higher K_1 ³⁵:

$$K_1 = \frac{4 k_B T}{\pi D} \phi \frac{\bar{L}}{D} \quad (12)$$

Here we introduced a new notation \bar{L} for the characteristic (average) length of aggregates. Using this expression and the values of $K_1 = 5 \text{ pN}$, $\phi = 0.1$, $D = 1.6 \text{ nm}$ for $c = 14 \text{ wt\%}$ DSCG at $T = 297 \text{ K}$ (3K below T_{ni}), we find $\bar{L} \approx 25 \text{ nm}$, which compares well with a previous estimate⁵⁸ $\bar{L} = 18 \text{ nm}$ for the isotropic phase of the same concentration at 305K (5K above T_{ni}).

The twist elastic constant K_2 in the model of flexible rods is predicted to be⁴⁷

$$K_2 = \frac{k_B T}{D} \phi^{1/3} \left(\frac{\lambda_p}{D} \right)^{1/3} \quad (13)$$

implying a rather weak dependency on λ_p and ϕ . The smallness of K_2 and its independence of the contour length \bar{L} in LCLCs can be explained as follows⁸, Fig. 6(C). Consider an ideal arrangement of the aggregates in layers to accommodate a twisted director field. Within each layer, the aggregates are straight and closely packed; the direction of director is changed by a small angle only when moving between consecutive layers. Successive layers of aggregates simply stack on top of each other to form a twisted nematic distortion with $\mathbf{n} \perp$ helical axis. However, in reality, the aggregates cannot perfectly remain in the layers; for example, thermal fluctuations will displace the aggregates across layers and thus cause them to interfere with aggregates that have a different orientation. This interference can be relieved by bending the aggregates to conform to the local orientational order in the layer, instead of being aggravated by the extended aggregate length. Thus K_2 is

independent of \bar{L} and weakly dependent on λ_p (as compared to the bend elasticity K_3). From Eqs.(10) and (13), for typical values $\phi = 0.1$, $\lambda_p = 50$ nm, $D = 1.6$ nm, we deduce

$$\frac{K_2}{K_3} = \frac{\pi}{4} \left(\phi \frac{\lambda_p}{D} \right)^{-2/3} \approx 0.37, \text{ which qualitatively agrees with our}$$

argument that K_2 has weak dependence on λ_p , but still does not quantitatively explain the smallness of the observed ratio (K_2/K_3 in the range of 0.025-0.04 for all concentrations and temperatures). Clearly, an improved theory is needed.

Similarly to our previous study of SSY²⁷, K_1 and the ratio K_1/K_3 in DSCG decreases as the temperature increases, Fig 4. As follows from Eqs. (10) and (12) for the model of flexible aggregates, the ratio is:

$$\frac{K_1}{K_3} = \frac{\bar{L}}{\lambda_p} \quad (14)$$

The observed temperature dependence of K_1/K_3 cannot be explained by the Onsager-type models either for rigid rods or for flexible rods, if the mean aggregate length \bar{L} remains constant. Instead, as we now argue, different temperature dependences of the aggregate contour length \bar{L} and persistence length λ_p are responsible, a possibility which is absent in LCs with a fixed, temperature-independent shape of building units.

Consider \bar{L} first. Theoretical works suggest that \bar{L} depends on volume fraction ϕ , temperature T and scission energy E_a ^{1, 7, 8, 27, 55}. Compared to the expression for \bar{L} in a dilute ($\phi \ll 1$) isotropic phase, $\bar{L} = L_0 \sqrt{\phi} \exp\left(\frac{E_a}{2k_B T}\right)$, the form of \bar{L} in the nematic state exhibits a stronger dependence on ϕ due to the orientational order²⁷:

$$\bar{L} = L_0 \phi^{5/6} \left(\frac{\lambda_p}{D} \right)^{1/3} \exp\left(\frac{E_a + \sigma\phi}{2k_B T}\right) \quad (14)$$

Here $L_0 = 2\pi^{-2/3} \sqrt{a_z D}$ is a length characterizing the size of a monomer, a_z the period of molecular stacking along the aggregate, and σ a constant describing the enhancement of aggregation by the excluded volume effects. (In the second virial approximation⁵⁹, $\sigma \approx 4k_B T$.) For DSCG, $D = 1.6$ nm, $a_z = 0.34$ nm⁶⁰, $L_0 = 0.7$ nm. Using Eq. (12) for K_1 , we estimate that \bar{L} is in the range of (20-270) nm, and $E_a(\phi, T) \approx (8-14)k_B T$, close to the estimates for SSY LCLC by Collings et al⁶¹, $E_a \approx 7k_B T$, and by Day et al⁶², $E_a \approx 11k_B T$, and for DNA oligomers⁹ by Clark et al, $E_a \approx (4-8)k_B T$. To make contact

with the empirical expression above for K_1 in Eq.(7), we expand $\frac{E_a(\phi, T)}{k_B T}$ near $T_{ni} \approx 300$ K as follows:

$$\frac{E_a(\phi, T)}{k_B T} = \frac{E_a(\phi, T_{ni})}{k_B T_{ni}} - \left(\frac{E_a}{k_B T} - \frac{\partial E_a}{k_B \partial T} \right)_{T_{ni}} \frac{1}{T_{ni}} (T - T_{ni}) + O(T - T_{ni})^2 \quad (14)$$

This gives (to lowest order in $T - T_{ni}$):

$$\bar{L} \propto \exp \left[- \left(\frac{E_a}{k_B T} - \frac{\partial E_a}{k_B \partial T} \right)_{T_{ni}} \frac{T}{2T_{ni}} \right] \quad (14)$$

Inserting this result into Eq. (12) and comparing to Eq.(7), we identify $\beta_K = \frac{1}{2T_{ni}} \left(\frac{E_a}{k_B T} - \frac{\partial E_a}{k_B \partial T} \right)_{T_{ni}}$. Then using the experimental value of $\beta_K = 0.2 \pm 0.01$ K⁻¹ and the above estimates for $E_a(\phi, T)/k_B T \sim 10$ we find:

$$\frac{\partial E_a}{k_B \partial T} \Big|_{T_{ni}} = \frac{E_a}{k_B T_{ni}} - 2\beta_K T_{ni} < 0 \quad (14)$$

and therefore conclude that $E_a(\phi, T)$ decreases with increasing T .

As shown by numerical simulations⁵¹, the persistence length λ_p scales with ϕ and T as $\frac{\lambda_p}{L_0} \propto \frac{E_a(\phi, T)}{k_B T}$, and thus has a much

weaker dependence on ϕ (mainly through ionic effects) and T than does \bar{L} for chromonic aggregates formed by cylindrical monomers. From Eqs.(10), (12), and (14), we can deduce

$$\frac{K_1}{K_3} \propto \phi^{5/6} \exp\left(\frac{E_a + \kappa\phi}{2k_B T}\right) \left(\frac{E_a}{k_B T}\right)^{-2/3} \quad (14)$$

This equation implies that $\frac{K_1}{K_3}$ decreases when T increases or ϕ decreases, consistent with our measurements, Fig 4(A). Our experimental values of $\frac{K_1}{K_3}$ suggest that $\frac{\bar{L}}{\lambda_p}$ is in the range of (0.25-1.2), depending on T and ϕ . Interestingly, the numerical results of Kuriabova et al⁵¹, $L/\lambda_p \approx 1$, fall in this range.

The exponential dependence of K_1 on $\frac{E_a}{k_B T}$ and the weak dependence of K_2 on λ_p , Eq.(13), predict that $\frac{K_1}{K_2} \propto \phi^{3/2} \exp\left(\frac{E_a + 2\kappa\phi}{k_B T}\right)$ increases when T decreases or ϕ decreases, again consistent with our measurements, Fig. 4(B).

Regarding $\frac{K_3}{K_2}$, Eqs. (10) and (13) indicate

$\frac{K_3}{K_2} \propto \phi^{2/3} \left(\frac{\lambda_p}{D} \right)^{2/3} \propto \phi^{2/3} \left(\frac{E_a}{k_B T} \right)^{2/3}$. As temperature T decreases (ΔT increases), λ_p and $\frac{E_a}{k_B T}$ increase, thus $\frac{K_3}{K_2}$ should increase.

However, experiments show that $\frac{K_3}{K_2}$ remains practically

constant over a wide range of temperature for all studied ϕ , and that in fact it decreases at $T \approx 294\text{K}$ for the highest volume fraction $\phi = 0.129$ ($c = 18$ wt%), Fig 4(C). Apparently, some additional factor must account for this behaviour. One possibility is the following. For the $c = 18$ wt% sample at $T \approx 291\text{K}$ (3K below our experimental range), the system transforms into a columnar phase³⁹. In this phase, twist deformations are severely inhibited by the hexagonal packing of the long aggregates, and consequently $K_2 \rightarrow \infty$ is expected. A pretransitional increase of K_2 would explain the decrease in

$\frac{K_3}{K_2}$ seen at low temperatures in Fig 4(C).

B. Viscosities

The large values of the splay and twist viscosities measured in the DSCG LCLC, and the relatively small value of the bend viscosity, can be understood following the arguments put forward by de Gennes⁶³ and Meyer^{8, 33, 34, 36} for nematic LC polymers in the “infinite” chain limit, $\bar{L}/D \rightarrow \infty$. In this limit, twisting the director field is associated with mass displacement of single chains, which produces flows perpendicular to the director with a gradient along the director. If the chains are not allowed to break, twist deformation, even though conceptually possible as a static state as we argued earlier, is forbidden as a dynamic process since it induces flows that tend to cut the chains; as a result $\eta_{twist} = \gamma_1 \rightarrow \infty$, where γ_1 is the rotation viscosity of the director field⁴⁰. In a practical system with a finite (but still large) $\bar{L}/D \gg 1$, η_{twist} must increase as \bar{L} increases. A simple geometric argument due to Meyer^{8, 36} shows that $\eta_{twist} = \gamma_1 \propto \bar{L}^2$, Fig 6(D). Consider a twist deformation that induces shear flow $\frac{\partial v}{\partial z} = \text{const}$. The power

dissipated per monomer along the aggregates is $P = \mu \delta^2 \left(\frac{\partial v}{\partial z} \right)^2$,

where μ is a friction coefficient and δ is the distance of the monomer to the rotation centre. The mean power dissipation

$\bar{P} = \frac{1}{L} \int_{-\bar{L}/2}^{\bar{L}/2} P dz = \mu \frac{\bar{L}^2}{12} \left(\frac{\partial v}{\partial z} \right)^2$; thus the effective viscosity for the

twist process is $\eta_{twist} \propto \bar{L}^2$. A similar analysis applies to splay deformation, giving $\eta_{splay} \propto \bar{L}^2$. These predictions are consistent with our experimental results for the η 's and with the linear

dependence $K_1 \propto \bar{L}$. Namely, as indicated in Fig. 3(A) and Fig. 5(A)(B): $K_1 \propto \exp(-\beta_K T)$ with $\beta_K = 0.20 \pm 0.01 \text{ K}^{-1}$; $\eta_{twist} \propto \exp(-\beta_t T)$ with $\beta_t = 0.37 \pm 0.01 \text{ K}^{-1}$; and $\eta_{splay} \propto \exp(-\beta_s T)$ with $\beta_s = 0.41 \pm 0.02 \text{ K}^{-1}$. The result $\beta_t \approx \beta_s \approx 2\beta_K$ agrees with the theoretical scaling relations, $K_1, \eta_{splay}^{1/2}, \eta_{twist}^{1/2} \propto \bar{L}$, and the temperature dependence of the viscoelastic parameters predicted by Eq. (14) in the vicinity of T_{ni} is also confirmed.

The viscosity associated with bend deformation, η_{bend} is comparable to values for thermotropic LCs, Table 1, and is several orders of magnitude smaller than η_{splay} and η_{twist} . This is explained by the fact that bend deformation is associated with “sliding” the aggregates parallel to each other^{8, 34-36}, which is not inhibited even if \bar{L}/D becomes very large.

An important difference in the hydrodynamic properties of LCLCs relative to those of low-molecular LCs is illustrated in Fig. 5(D), which shows the temperature dependence of $\eta_{splay}/\eta_{twist}$. In DSCG, this ratio is close to but still somewhat larger than 1. The result is unusual from the point of view of the Ericksen-Leslie model⁴⁰, in which the twist viscosity $\eta_{twist} = \gamma_1$ is always larger than splay viscosity $\eta_{splay} = \gamma_1 - \frac{\alpha_3^2}{\eta_b}$. (Here α_3 is one of the Ericksen-Leslie coefficients⁴⁰, and $\eta_b > 0$ is one of the Miezwicz viscosities⁴⁰.) Our experimental results, Fig 5(D), however, show that $\eta_{splay}/\eta_{twist} \approx 1$ holds only in the vicinity of the transition to the isotropic phase. When ΔT increases and the system moves deeper into nematic phase, $\eta_{splay}/\eta_{twist}$ can be as large as 2. This finding suggests that the explanation of the anomalous behaviour seen in Fig. 5(D) is again rooted in the strong temperature and concentration dependencies of the mean aggregate length \bar{L} .

C. Origin of the additional fluctuation mode in the bend geometry

Finally, we discuss the origin of the additional fluctuation mode (\bar{I}_4, Γ_4) detected in the bend scattering geometry. The key features of this mode are: (1) it is hydrodynamic ($\Gamma_4 \propto q_0^2$); (2) it couples weakly to light (\bar{I}_4 is ~ 10 times smaller than \bar{I}_3 for the director bend mode); and (3) it is ~ 10 times slower than the bend fluctuations but $\sim 10^2 - 10^3$ times faster than splay or twist.

We propose that the additional mode is associated with the thermal diffusion of structural defects in the chromonic aggregates. To establish this conjecture, we point out the following. The plank-like chromonic molecules tend to aggregate face-to-face, to shield the exposure of extended aromatic cores to water. The scission energy E_a of this non-covalent association is about $10k_B T$ as shown in our analysis above and references^{9, 61, 62}. The molecular association might therefore form metastable configurations that do not correspond to the absolute minimum of the interaction potential. For example, the association might happen with a lateral shift or rotation of the molecular planes. Some of these defects or their combinations alter the aggregate structure so significantly that they impose deformations on the surrounding director field. As illustrated in Fig. 7, a pair of lateral shifts, which we call a “C” defect, tends to impose a bend deformation ($\hat{\mathbf{n}} \times \text{curl} \hat{\mathbf{n}}$) on the director $\hat{\mathbf{n}}$. A sequence of such “C” defects can be pictured as a crankshaft. On the other hand, a junction of three aggregates, with the symmetry of the letter “Y”, creates a different type of defect that imposes a splay distortion ($\hat{\mathbf{n}} \text{div} \hat{\mathbf{n}}$) on the director field, Fig. 7. The presence of both defect types has already been suggested to explain a discrepancy between the length of chromonic aggregates expected from the point of view of the Onsager model of lyotropic mesomorphism and the length inferred from X ray scattering data⁶⁰. Interestingly, recent structural studies of sunset yellow support the existence of stacking features in the form of lateral shifts⁶⁴.

The stacking defects illustrated in Fig. 7 are polar. To incorporate their thermal diffusion into a description of the orientational fluctuation modes, we let the j -th type of polar defect be described by the vector density $\mathbf{v}_j(\mathbf{r})$. For example, $j = 1$ for “C” type, and $j = 2$ for “Y” type, Fig. 7. The effect of the defect dynamics on the light scattering is caused by their interaction with director distortions. This interaction, which may be termed flexopolarity, results in additional symmetry-allowed cross terms in the Frank elastic free energy. These terms couple the distortion vector $\mathbf{G}(\mathbf{r}) = g_s \hat{\mathbf{n}} \text{div} \hat{\mathbf{n}} + g_b (\hat{\mathbf{n}} \times \text{curl} \hat{\mathbf{n}})$, where g_s and g_b are splay and bend flexopolar coefficients, respectively, to the vector density \mathbf{v}_j . Additionally, in the free energy we must consider an interaction between defects that penalizes fluctuations in their concentration. Generally, this may be expressed by a tensor coupling of the form $\mathbf{v} \cdot \mathbf{h} \cdot \mathbf{v}$, where the tensor core $h_{jk}(\mathbf{r}-\mathbf{r}')$ defines the energy penalty for the polar defect densities and also ensures positivity of the free energy. To simplify the analysis, we neglect the interaction between different defect types and thus take $h_{jk}(\mathbf{r}-\mathbf{r}') = h_j(\mathbf{r}-\mathbf{r}')\delta_{jk}$. Based on these considerations, the free energy becomes:

$$F = \int \left[f_{FO} + \sum_j \mathbf{v}_j(\mathbf{r}) \cdot \mathbf{G}(\mathbf{r}) \right] d\mathbf{r} + \frac{1}{2} \int \sum_j \mathbf{v}_j(\mathbf{r}) \cdot \mathbf{h}_j(\mathbf{r}-\mathbf{r}') \cdot \mathbf{v}_j(\mathbf{r}') d\mathbf{r} d\mathbf{r}' \quad (15)$$

where $f_{FO} = \frac{1}{2} [K_1 (\text{div} \hat{\mathbf{n}})^2 + K_2 (\hat{\mathbf{n}} \cdot \text{curl} \hat{\mathbf{n}})^2 + K_3 (\hat{\mathbf{n}} \times \text{curl} \hat{\mathbf{n}})^2]$ is the standard Frank-Oseen bulk elastic energy⁴⁰.

Using the Fourier transform $\mathbf{v}_j(\mathbf{r}) = V^{-1} \sum_{\mathbf{q}} \mathbf{v}_j(\mathbf{q}) \exp(i\mathbf{q} \cdot \mathbf{r})$ and the standard quadratic representation for director fluctuation modes around the equilibrium director $\hat{\mathbf{n}}_0$, $\hat{\mathbf{n}}(\mathbf{r}) = \hat{\mathbf{n}}_0 + V^{-1} \sum_{\mathbf{q}} \sum_{\alpha=1,2} n_{\alpha}(\mathbf{q}) \hat{\mathbf{e}}_{\alpha} \exp(i\mathbf{q} \cdot \mathbf{r})$ in the frame $\{\hat{\mathbf{e}}_1, \hat{\mathbf{e}}_2, \hat{\mathbf{n}}_0\}$, where $\mathbf{q} = q_{\perp} \hat{\mathbf{e}}_1 + q_{\parallel} \hat{\mathbf{n}}_0$, we obtain

$$F = \frac{1}{2V} \sum_{\mathbf{q}} \left\{ (K_{\alpha} q_{\perp}^2 + K_3 q_{\parallel}^2) |n_{\alpha}(\mathbf{q})|^2 + 2ig_s q_{\perp} v_{j\perp}^*(\mathbf{q}) n_1(\mathbf{q}) - 2ig_b q_{\parallel} v_{j\alpha}^*(\mathbf{q}) n_{\alpha}(\mathbf{q}) + h_j^{\square}(\mathbf{q}) |v_{j\perp}(\mathbf{q})|^2 + h_j^{\square}(\mathbf{q}) |v_{j\alpha}(\mathbf{q})|^2 \right\} \quad (15)$$

where $v_j(\mathbf{q}) = v_{j1} \hat{\mathbf{e}}_1 + v_{j2} \hat{\mathbf{e}}_2 + v_{j\parallel} \hat{\mathbf{n}}_0$, summation is performed in Eq. (15) over indices j , and $\alpha = 1, 2$ in the terms where they appear. Due to uniaxial anisotropy with respect to $\hat{\mathbf{n}}_0$, the tensors $h_j(\mathbf{q}) = \int h_j(\bar{\mathbf{r}} = \mathbf{r}-\mathbf{r}') \exp(-i\mathbf{q} \cdot \bar{\mathbf{r}}) d\bar{\mathbf{r}}$ are diagonal with components $h_j^{\square}(\mathbf{q})$ and $h_j^{\perp}(\mathbf{q})$ being parallel and perpendicular to $\hat{\mathbf{n}}_0$, respectively. We consider the polar defect mode ($j\beta$), $\beta = 1, 2, \square$, as a ‘fast’ or ‘slow’ mode, depending on the magnitude of its relaxation rate $\Gamma_{j\beta}$ compared to the relaxation rate Γ_{α}^n of the director distortions $n_{\alpha}(\mathbf{q})$.

Fast defect regime ($\Gamma_{j\beta} \gg \Gamma_{\alpha}^n$): When the director fluctuations are slow compared to the defect modes, their effect on the defect densities $v_{j\alpha}$ results in quasi-equilibrium values, $\tilde{v}_{j\alpha}(\mathbf{q}) = ig_b q_{\parallel} n_{\alpha}(\mathbf{q}) / h_j^{\perp}(\mathbf{q})$ and $\tilde{v}_{j\perp}(\mathbf{q}) = ig_s q_{\perp} n_1(\mathbf{q}) / h_j^{\square}(\mathbf{q})$, determined by the minimization of F , Eq. (15), over $v_{j\alpha}^*(\mathbf{q})$ and $v_{j\perp}^*(\mathbf{q})$. This “instantaneous” response effectively renormalizes the elastic constants for ‘spontaneous’ director fluctuations

$$K_1 \rightarrow K_1 - \sum_j g_s^2 / h_j^{\square}(\mathbf{q}), \quad K_3 \rightarrow K_3 - \sum_j g_b^2 / h_j^{\perp}(\mathbf{q}) \quad (16)$$

where the summation is over the fast defect modes. Except for this effect on the elastic moduli, “fast” defect modes are almost invisible in the DLS experiment probing director fluctuations. This fact is consistent with the lack of evidence for an additional, defect mode in the splay+twist scattering geometry, where the observed director fluctuations are much slower than either of the modes detected in the bend geometry.

Slow defect regime ($\Gamma_{j\beta} \ll \Gamma_{\alpha}^n$): Here the defect diffusion modes serve as a slowly changing random force field, that creates the quasi-equilibrium, defect-induced director distortions, obtained by minimizing F , Eq. (15), over $n_{\alpha}(\mathbf{q})$:

$$\tilde{n}_{\alpha}(\mathbf{q}) = \sum_j \tilde{n}_{\alpha}^{(j)}(\mathbf{q}) = i \sum_j \frac{g_b q_{\parallel} v_{j\alpha}(\mathbf{q}) - g_s q_{\perp} v_{j\perp}(\mathbf{q})}{K_{\alpha} q_{\perp}^2 + K_3 q_{\parallel}^2} \quad (17)$$

where the summation is over slow defect modes.

The bend scattering geometry, where the director mode is relatively fast, is the most favourable situation for directly observing fluctuations of $v_{j\beta}$, and is indeed the case where we do detect an extra mode. With $\alpha = 2$ (corresponding to the twist-bend director mode) and $q_{\parallel} \ll q_{\perp}$ (corresponding to nearly pure bend), we see from Eq. (17) that the diffusive modes v_{j2} couple to the director mode with coupling strength controlled by the parameter g_b . Even if v_{j2} fluctuations are slower than the bend fluctuations, their contribution to scattering can be weak, provided g_b is small, and thus agree with the behaviour observed experimentally for the additional mode $(\bar{\Gamma}_4, \Gamma_4)$.

In principle, both translational and rotational diffusion of the polar defects could explicitly contribute to temporal variations of the defect density $\partial v_{j2} / \partial t$. However, when $q_{\perp} = 0$, the directions \hat{e}_1 and \hat{e}_2 in the plane perpendicular to \hat{n}_0 are equivalent, v_{j2} and v_{j1} are degenerate, and rotational diffusion does not directly change the defect density that couples to the director mode. However, translational diffusion along \hat{n}_0 can modulate v_{j2} (or v_{j1}) in regions of high or low bend distortion of the director. For $q = q_{\parallel}$ (as is essentially the case in the bend scattering geometry studied), we therefore expect a hydrodynamic mode with $\Gamma_{j2} \propto q_{\parallel}^2$, consistent with the experimental q dependence of Γ_4 .

The fact that the stretching parameter b used in stretched exponential fits of the correlation functions in the bend geometry (Eq.(9)) is ~ 0.9 rather than 1 (pure exponential) indicates that both bend deformation and thermal diffusion of the configuration defects are associated with slightly dispersed instead of single valued relaxation rates Γ_3 and Γ_4 . This could result from a geometric dispersion of stacking defects. Since the stacking of the DSCG molecules into aggregates is isodesmic⁶¹, there is no obvious preference for certain geometrical parameters, such as the length of the arms of the ‘‘C’’ or ‘‘Y’’ defects, to prevail over others. As a result of dispersed geometric parameters of the stacking defects, we would expect some dispersion in relaxation rates $\Gamma_{j\beta}$ and Γ_{α}^n (Eq. (9) and Fig. 2).

Conclusions

We have measured the temperature and concentration dependences of the orientational elastic moduli and corresponding viscosities for the lyotropic nematic phase of a self-assembled LCLC system. Over the (3-10) K nematic temperature range of $c = (12.5 - 18)$ wt% DSCG LCLCs,

$K_3 \approx K_1 \sim 10\text{pN}$, $K_2 \sim 1\text{pN}$, $\eta_{twist} \approx \eta_{splay} \sim (1 - 500) \text{kgm}^{-1}\text{s}^{-1}$ and $\eta_{bend} \approx 0.01 \text{kgm}^{-1}\text{s}^{-1}$. Of the three elastic constants, the splay constant (K_1) has the strongest temperature dependence, which is described by an exponential function of T . The twist and splay viscosities, η_{twist} and η_{splay} show similar exponential temperature dependences. We qualitatively explained these results by using the viscoelastic theory developed for LC systems formed by semi-flexible long chain particles with aspect ratio $\bar{L}/D \ll 1$ and by specifically confirming the predicted scaling of parameters, $K_1, \eta_{splay}^{1/2}, \eta_{twist}^{1/2} \propto \bar{L}$, with the strongly temperature-dependent average contour length \bar{L} . Our results demonstrating weak temperature dependence of the other parameters (K_2, K_3 , and η_{bend}) also agree with theory. We detect an additional fluctuation mode in the bend geometry, which we attributed to the thermal diffusion of structural defects of the chromonic aggregates. These features, absent in conventional thermotropic LCs and lyotropic polymer LCs, highlight the fact that in LCLC system, the building units are non-covalently bound aggregates rather than molecules of fixed size.

Acknowledgements

This work was supported by NSF Materials World Network on Lyotropic Chromonic Liquid Crystals, grant DMR076290, NSF DMR 1121288, by Samsung Electronics Corp., by Fundamental Research State Fund Project UU24/018 and by the Ministry of Education and Sciences of Ukraine, Project 0113U000468. We thank Dr. Bart Kahr for sending us the manuscript⁶⁴.

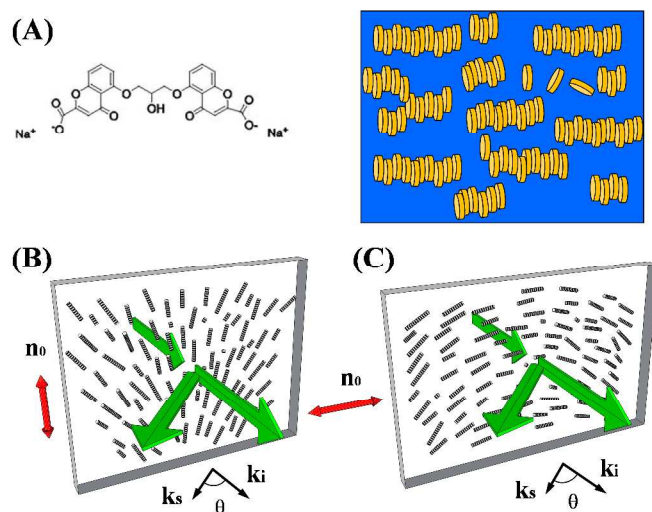


FIG. 1: (A) Structure of the DSCG molecule and generic representation of LCLC aggregates formed in aqueous solution. (Each disk in the aggregate stack may represent single or paired DSCG molecules.) (B)(C) Schematic of experimental light scattering geometries used in our measurements: (B) “1&2”, splay+twist (pure splay shown) geometry and (C) “3” bend-twist (pure bend shown) geometry.

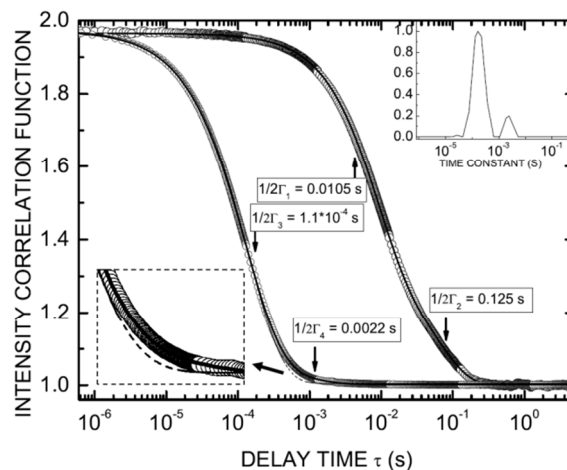


FIG. 2: Correlation functions (open circles) collected at $T = 294$ K for $q_{\parallel} = 1.64 \times 10^6 \text{ m}^{-1}$ in a bend (left) and for $q_{\perp} = 1.00 \times 10^7 \text{ m}^{-1}$ in splay + twist geometries (right) for the nematic LCLC formed by 14 wt % DSCG in water. Solid lines represent fits of the correlation functions (double exponential in the splay + twist geometry, stretched double exponential in bend geometry) to obtain relative normalized amplitudes I_{α} and relaxation rates Γ_{α} ($\alpha = 1 - 3$), of the fluctuation modes. In the bend geometry, the analysis reveals an additional, weak mode Γ_4 . In this case, the best single-exponential fit (the dashed line) clearly misses the data in the ($10^{-4} - 10^{-3}$) s region (left inset). The right inset shows the relaxation time spectrum obtained by the regularization method⁶⁵ for the bend geometry correlation function; the small secondary peak confirms the presence of the additional mode.

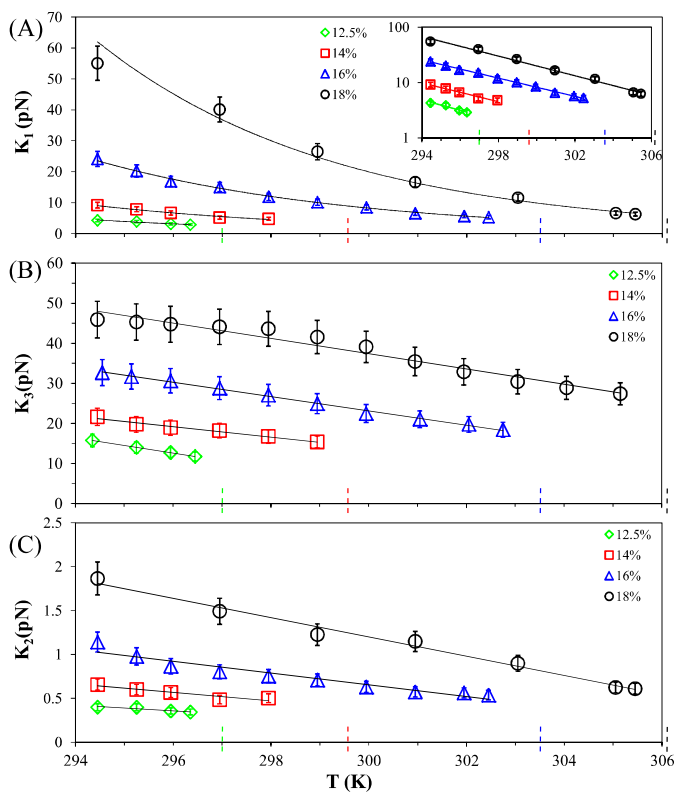


FIG. 3: (Colour online) Temperature and concentration dependences of elastic constants of (A)splay K_1 , (B)bend K_3 and (C)twist K_2 in nematic phase. Dashed vertical lines on the horizontal axes indicate the transition temperature from nematic to nematic-isotropic coexistence phase. The insert shows K_1 has an exponential dependence of temperature T . K_3 and K_2 fit well with linear functions of temperature T .

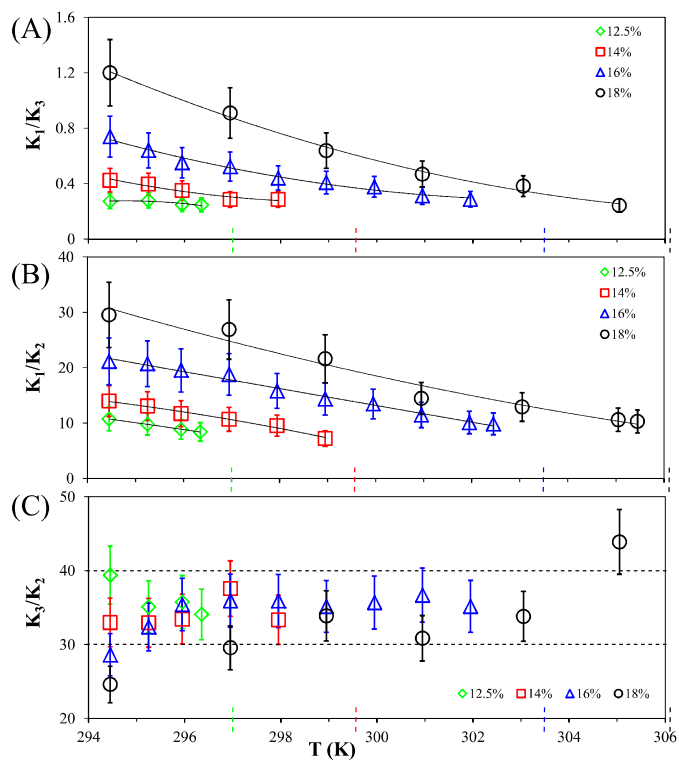


FIG. 4: (Colour online) Temperature and concentration dependences of the ratios between elastic constants. (A) K_1 / K_3 , (B) K_1 / K_2 both increase as T decreases or ϕ increases; (C) K_3 / K_2 remains practically constant for a wide range of T , but decreases at $T \approx 294\text{K}$ for 18 wt %.

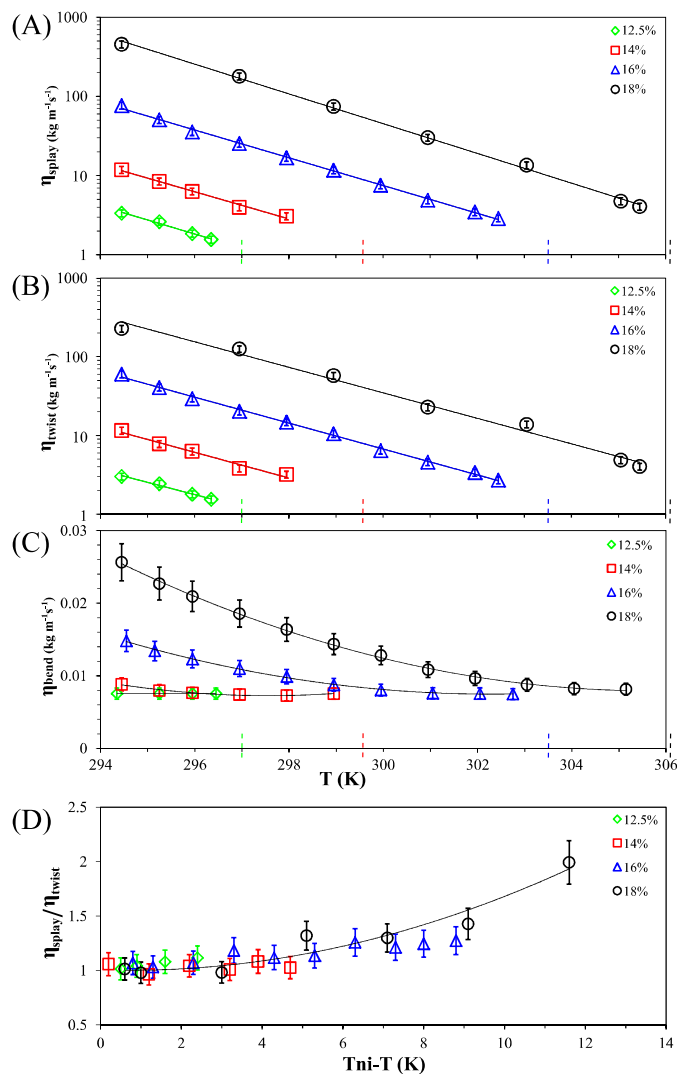


FIG. 5: Temperature and concentration dependences of viscosities and their ratios: (A) η_{splay} , (B) η_{twist} , (C) η_{bend} and (D) $\eta_{splay}/\eta_{twist}$ over the nematic range. Dashed lines in the horizontal axis indicate T_m .

LCs	K_1 (pN)	K_2 (pN)	K_3 (pN)	η_{splay} ($\text{kgm}^{-1}\text{s}^{-1}$)	η_{twist} ($\text{kgm}^{-1}\text{s}^{-1}$)	η_{bend} ($\text{kgm}^{-1}\text{s}^{-1}$)
DSCG	10.2	0.7	24.9	11.7	10.5	0.009
SSY	4.3	0.7	6.1	-	-	-
PBG	7.5	0.6	6	2.5	2.5	0.025
5CB	4.5	3	5.5	0.088	0.094	0.015

TAB. 1: Viscoelastic parameters of different liquid crystals. LCLC DSCG: 16 wt%, $\phi = 0.115$, $\Delta T = 4.3\text{K}$; LCLC SSY: 29 wt%, $\phi = 0.20$, $\Delta T = 2\text{K}$; lyotropic polymeric LC PBG: $L/D = 32$, $\phi = 0.16$; thermotropic LC 5CB: $\Delta T = 4\text{K}$.

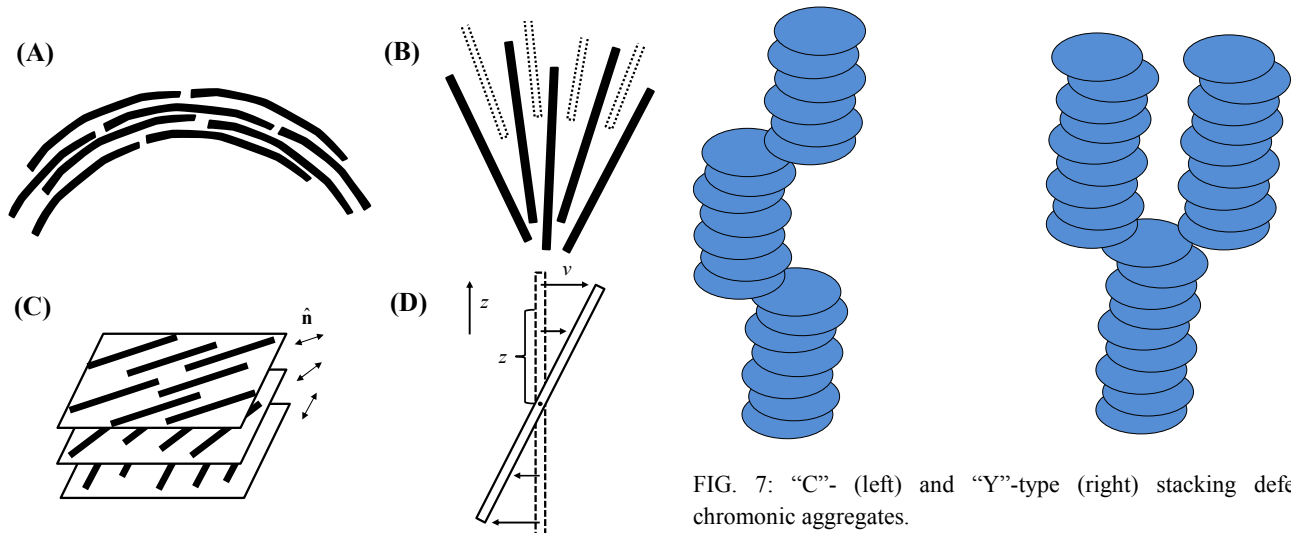


FIG. 7: "C"- (left) and "Y"-type (right) stacking defects in chromonic aggregates.

FIG. 6: Mechanism of viscoelastic processes in LCLC, following Meyer et al.⁸. (A) Flexible rods accommodate bend deformation by deforming the rods. (B) Splay deformation tends to create vacancies that require free ends (marked by dashed lines) to fill in. (C) Twist deformation causes minimum inter-aggregate interference by arranging aggregates in layers. (D) Shear flow associated with twist deformation.

Notes and references

^a Liquid Crystal Institute, Kent State University, Kent, OH 44242 USA.

^b Chemical Physics Interdisciplinary Program, Kent State University, Kent, OH 44242 USA.

^c Department of Physics, Kent State University, Kent, OH, 44242 USA.

^d Institute of Physical Optics, 23 Dragomanov str., Lviv, 79005, Ukraine.

* Current address: Department of Physics, University of Alberta, Edmonton, Alberta T6G 2G7, Canada.

† Electronic address: olavrent@kent.edu

‡ Electronic address: ssprunt@kent.edu

1. J. Lydon, *Liquid Crystals*, 2011, **38**, 1663-1681.
2. P. J. Collings, A. J. Dickinson and E. C. Smith, *Liquid Crystals*, 2010, **37**, 701-710.
3. S.-W. Tam-Chang and L. Huang, *Chemical Communications*, 2008, 1957-1967.
4. D. J. Edwards, A. P. Ormerod, G. J. T. Tiddy, A. A. Jaber and A. Mahendrasingham, in *Physico-Chemical Principles of Color Chemistry*, eds. A. T. Peters and H. S. Freeman, Springer Netherlands, 1996, vol. 4, ch. 3, pp. 83-106.
5. A. S. Vasilevskaya, E. V. Generalova and S. S. Anatolii, *Russian Chemical Reviews*, 1989, **58**, 904.
6. F. Guo and R. Hurt, *Macromolecular Chemistry and Physics*, 2012, **213**, 1164-1174.
7. P. v. der Schoot and M. E. Cates, *Langmuir*, 1994, **10**, 670-679.
8. R. B. Meyer, *Polymer Liquid Crystals*, Academic Press, New York, 1982.
9. M. Nakata, G. Zanchetta, B. D. Chapman, C. D. Jones, J. O. Cross, R. Pindak, T. Bellini and N. A. Clark, *Science*, 2007, **318**, 1276-1279.
10. H. S. Park and O. D. Lavrentovich, *Lyotropic Chromonic Liquid Crystals: Emerging Applications* John Wiley & Sons, Hoboken, New Jersey, 2012.
11. M. E. Sousa, S. G. Cloutier, K. Q. Jian, B. S. Weissman, R. H. Hurt and G. P. Crawford, *Applied Physics Letters*, 2005, **87**, -.
12. S.-W. Tam-Chang, J. Helbley, T. D. Carson, W. Seo and I. K. Iverson, *Chemical Communications*, 2006, 503-505.
13. Y. Yi and N. A. Clark, *Liquid Crystals*, 2013, **40**, 1736-1747.
14. M. A. Lohr, M. Cavallaro, D. A. Beller, K. J. Stebe, R. D. Kamien, P. J. Collings and A. G. Yodh, *Soft Matter*, 2014, **10**, 3477-3484.
15. T. Schneider and O. D. Lavrentovich, *Langmuir*, 2000, **16**, 5227-5230.
16. C. M. Tone, M. P. De Santo, M. G. Buonomenna, G. Golemme and F. Ciuchi, *Soft Matter*, 2012, **8**, 8478-8482.
17. V. G. Nazarenko, O. P. Boiko, H. S. Park, O. M. Brodyn, M. M. Omelchenko, L. Tortora, Y. A. Nastishin and O. D. Lavrentovich, *Physical Review Letters*, 2010, **105**, 017801.
18. N. Ould-Moussa, C. Blanc, C. Zamora-Ledezma, O. D. Lavrentovich, I. I. Smalyukh, M. F. Islam, A. G. Yodh, M. Maugey, P. Poulin, E. Anglaret and M. Nobili, *Liquid Crystals*, 2013, **40**, 1628-1635.
19. Y. A. Nastishin, H. Liu, T. Schneider, V. Nazarenko, R. Vasyuta, S. V. Shiyonovskii and O. D. Lavrentovich, *Physical Review E*, 2005, **72**, 041711.
20. Y.-K. Kim, S. V. Shiyonovskii and O. D. Lavrentovich, *Journal of Physics: Condensed Matter*, 2013, **25**, 404202.
21. L. Tortora and O. D. Lavrentovich, *Proceedings of the National Academy of Sciences of the United States of America*, 2011, **108**, 5163-5168.
22. J. Jeong, Z. S. Davidson, P. J. Collings, T. C. Lubensky and A. G. Yodh, *Proceedings of the National Academy of Sciences of the United States of America*, 2014, **111**, 1742-1747.
23. X. Yao, Doctor of Philosophy, Georgia Institute of Technology, 2011.
24. R. B. Meyer, F. Lonberg, V. Taratuta, S. Fraden, S.-D. Lee and A. J. Hurd, *Faraday Discuss. Chem. Soc.*, 1985, **79**, 125-132.
25. A. V. Golovanov, A. V. Kaznacheev and A. S. Sonin, *Izvestiya Akad. Nauk, Ser. Fiz.*, 1995, **59**, 82.
26. A. V. Golovanov, A. V. Kaznacheev and A. S. Sonin, *Izvestiya Akad. Nauk, Ser. Fiz.*, 1996, **60**, 43.
27. S. Zhou, Y. A. Nastishin, M. M. Omelchenko, L. Tortora, V. G. Nazarenko, O. P. Boiko, T. Ostapenko, T. Hu, C. C. Almasan, S. N. Sprunt, J. T. Gleeson and O. D. Lavrentovich, *Physical Review Letters*, 2012, **109**, 037801.
28. J. Jeong, G. Han, A. T. C. Johnson, P. J. Collings, T. C. Lubensky and A. G. Yodh, *Langmuir*, 2014, **30**, 2914-2920.
29. S. V. Shiyonovskii, T. Schneider, I. I. Smalyukh, T. Ishikawa, G. D. Niehaus, K. J. Doane, C. J. Woolverton and O. D. Lavrentovich, *Physical Review E*, 2005, **71**, 020702.
30. A. Kuma, T. Galstian, S. K. Pattanayek and S. Rainville, *Mol. Cryst. Liq. Cryst.*, 2013, **574**, 33-39.
31. Peter C. Mushenheim, Rishi R. Trivedi, Hannah H. Tuson, Douglas B. Weibel and Nicholas L. Abbott, *Soft Matter*, 2014, **10**, 88-95.
32. S. Zhou, A. Sokolov, O. D. Lavrentovich and I. S. Aranson, *Proceedings of the National Academy of Sciences of the United States of America*, 2014, **111**, 1265-1270.
33. V. G. Taratuta, A. J. Hurd and R. B. Meyer, *Phys. Rev. Lett.*, 1985, **55**, 246.
34. S.-D. Lee and R. B. Meyer, *Liq. Cryst.*, 1990, **7**, 15-29.
35. V. G. Taratuta, F. Lonberg and R. B. Meyer, *Phys. Rev. A*, 1988, **37**, 1831.
36. S.-D. Lee and R. B. Meyer, *Phys. Rev. Lett.*, 1988, **61**, 2217
37. Y. A. Nastishin, K. Neupane, A. R. Baldwin, O. D. Lavrentovich and S. Sprunt, *electronic-Liquid Crystal Communications*, 2008.
38. Y. A. Nastishin, K. Neupane, A. R. Baldwin, O. D. Lavrentovich and S. Sprunt, *arXiv:0807.2669*, 2008.
39. Hartshorn.Nh and G. D. Woodard, *Molecular Crystals and Liquid Crystals*, 1973, **23**, 343-368.
40. P. G. de Gennes and J. Prost, *The Physics of Liquid Crystals*, Clarendon Press, Oxford, 1993.
41. P. P. Karat and N. V. Madhusudana, *Mol. Cryst. Liq. Cryst.*, 1977, **40**, 239-245.
42. T. Toyooka, G.-P. Chen, H. Takezoe and A. Fukuda, *Jap. J. Appl. Phys.*, 1987, **26**, 1959-1966.
43. M. Cui and J. R. Kelly, *Mol. Cryst. Liq. Cryst.*, 1999, **331**, 49-57.
44. B. J. Berne and R. Pecora, *Dynamic Light Scattering*, Wiley, New York, 1976.
45. M. N. Berberan-Santos, E. N. Bodunov and B. Valeur, *Chemical Physics*, 2005, **315**, 171182.
46. G. J. Vroege and T. Odijk, *J. Chem. Phys.*, 1987, **87**, 4223.
47. T. Odijk, *Liq. Cryst.*, 1986, **1**, 553-559.
48. A. Y. Grosberg and A. V. Zhestkov, *Polymer Sci. USSR*, 1986, **28**, 97.
49. L. Tortora, H. S. Park, S. W. Kang, V. Savaryn, S. H. Hong, K. Kaznatcheev, D. Finotello, S. Sprunt, S. Kumar and O. D. Lavrentovich, *Soft Matter*, 2010, **6**, 4157-4167.
50. F. Chami and M. R. Wilson, *J. Am. Chem. Soc.*, 2010, **132**, 7794-7802.
51. T. Kuriabova, M. D. Betterton and M. A. Glaser, *J. Mater. Chem.*, 2010, **20**, 10366.
52. H. Cachitas, P. J. Sebastião, G. Feio and F. V. Chávez, *Liquid Crystals*, 2014, **accepted**.
53. L. D. Landau and E. M. Lifshitz, *Statistical Physics*, Pergamon Press, 1980.
54. L. D. Landau and E. M. Lifshitz, *Theory of Elasticity*, Butterworth-Heinemann, Oxford, 1986.
55. A. J. Dickinson, N. D. LaRacuenta, C. B. McKitterick and P. J. Collings, *Molecular Crystals and Liquid Crystals*, 2009, **509**, 751-762.
56. M. Hogan, J. LeGrange and B. Austin, *Nature*, 1983, **304**, 752-754.
57. S. B. Smith, Y. Cui and C. Bustamante, *Science*, 1996, **271**, 795-799.
58. Y. A. Nastishin, H. Liu, S. V. Shiyonovskii, O. D. Lavrentovich, A. F. Kostko and M. A. Anisimov, *Physical Review E*, 2004, **70**, 051706.
59. P. v. der Schoot and M. E. Cates, *Europhys. Lett.*, 1994, **25**, 515.

60. H. S. Park, S. W. Kang, L. Tortora, Y. Nastishin, D. Finotello, S. Kumar and O. D. Lavrentovich, *Journal of Physical Chemistry B*, 2008, **112**, 16307-16319.
61. V. R. Horowitz, L. A. Janowitz, A. L. Modic, P. A. Heiney and C. P. J., *Phys. Rev. E*, 2005, **72**, 041710.
62. M. P. Renshaw and I. J. Day, *J. Phys. Chem. B*, 2010, **114**, 10032–10038.
63. P. G. de Gennes, *Polymer Liquid Crystals*, Academic Press, New York, 1982.
64. W. Xiao, C. Hu, D. J. Carter, S. Nichols, M. D. Ward, P. Raiteri, A. L. Rohl and B. Kahr, *submitted*, 2014.
65. S. W. Provencher, *Comput. Phys. Commun.*, 1982, **27**, 213-229.